Icarus xxx (2013) xxx–xxx

Contents lists available at SciVerse ScienceDirect

Icarus

journal homepage: www.elsevier.com/locate/icarus

Inverse maximum gross bedform-normal transport 1: How to determine a dune-constructing wind regime using only imagery

Lori K. Fenton [a,*], Timothy I. Michaels [a], Ross A. Beyer [a,b]

[a] SETI Institute, 189 Bernardo Ave., Suite 100, Mountain View, CA 94043, USA
[b] NASA Ames Research Center, Moffett Field, CA 94035, USA

ARTICLE INFO

Article history:
Available online xxxx

Keywords:
Mars, Atmosphere
Geological processes
Meteorology
Image processing

ABSTRACT

It has been a goal of aeolian science to use bedforms as indicators of local and regional sediment transport and atmospheric circulation, but even with the application of the rule of maximum gross-bedform normal transport (MGBNT), the underdetermined nature of the problem has precluded its application in all but the most simple cases. We present a method to apply the rule of MGBNT and its inverse (IMGBNT) from analysis of aeolian dune crestlines derived from aerial imagery. Although the solutions to IMGBNT analysis are non-unique, the possible transport vectors influencing bedform morphology can often be constrained by making inferences regarding bedform type (e.g., transverse, oblique, or longitudinal), resultant drift direction, and the ratio of transport vector magnitudes. The technique is demonstrated on the Great Sand Dunes, located in Colorado, USA. This dune field has a wide array of dune morphologies; eight crestline sets were identified and mapped. IMGBNT analysis and the subsequent constraint of possible solutions suggests that transport vectors from the southeast and southwest, with a SE:SW transport ratio of ~1:2, produce oblique north–south oriented dunes that dominate the main dune field. These results compare favorably with MGBNT analysis of meteorologic measurements from three stations located adjacent to the Great Sand Dunes, which predict dune types and orientations similar to those observed in their vicinity.

1. Introduction

Aeolian bedforms have been identified on each of the four worlds in the Solar System which possess a substantial atmosphere and an observable surface (i.e., Venus, Earth, Mars, and Titan). Despite significant differences in the near-surface gravitational acceleration and atmospheric properties on these worlds, the processes leading to dune field construction are thought to be dynamically similar. This occurs because, like many other spatially repeating patterns in nature, dune fields are considered to be complex systems that exhibit self-organizing behavior (Werner, 1999). Although bedforms originate from saltation of individual grains, it is the interactions at the scale of the dune and dune field (e.g., dune collisions and defect migration) that drive pattern development (Werner and Kocurek, 1997; Elbelrhiti et al., 2005, 2008; Kocurek et al., 2010). In other words, the details of entrainment and transport for individual particles may vary from one environment to another, but large-scale processes remain similar. Pattern formation and development is governed by the boundary conditions imposed on the dune field, such as sediment availability, source-area geometry, and the areal limits of the dune field (Lancaster, 1999; Ewing and Kocurek, 2010a,b).

The boundary condition of relevance to this work is the aeolian wind regime (i.e., the relative directions and strengths of sand-transporting winds). It has long been known that wind patterns control dune morphology (e.g., Fryberger and Dean, 1979; Tsoar, 1983; Wasson and Hyde, 1983; Lancaster, 1989a; Sweet and Kocurek, 1990). Rubin and Hunter (1987) and Rubin and Ikeda (1990) quantified these ideas, introducing and testing the concept of maximum gross bedform-normal transport (MGBNT), which states that the orientation and type of bedform (e.g., transverse, oblique, or longitudinal) is determined solely by the wind regime. Put succinctly, given knowledge of the wind patterns in a region (e.g., from anemometer measurements, sand flux measurements, and/or output from atmospheric models), the dune types and orientations that emerge from this wind regime can be predicted.

The inverse problem to MGBNT (IMGBNT) is the one most often encountered in Earth and planetary sciences, in which the bedform pattern is known from imagery, but the incident sand-moving winds are not known. The solutions to IMGBNT are non-unique, but careful inferences regarding dune morphology and sand transport directions may be used to constrain the possible range of dune-forming winds. We present a practical application of MGBNT and

* Corresponding author.
E-mail address: lfenton@carlsagancenter.org (L.K. Fenton).

0019-1035/$ - see front matter © 2013 Elsevier Inc. All rights reserved.
http://dx.doi.org/10.1016/j.icarus.2013.04.001

IMGBNT that can be used on any imagery in which bedforms are resolved. This work seeks to improve on less sophisticated techniques of inferring wind direction (previously used by some of the authors); for example, assuming sand-moving winds are transverse to bedform orientations (e.g., Fenton et al., 2003; Hayward et al., 2007). These prior methods could not represent the full range of wind directions and were incapable of determining the relative strengths (transport ratios) of the various dune-building winds.

An understanding of the wind regime in remote locations, where direct atmospheric measurements are sparse or nonexistent, would greatly benefit from a practical application of this principle. It can be used to determine local weather patterns, which could affect the distribution of precipitation or ground water/ice stability (e.g., Hisatake et al., 1993; Chittenden et al., 2008). Determining major sand-transporting winds can also aid in the identification of aeolian sediment transport pathways, which are major agents of landscape evolution in arid climates. Inactive dunes could reflect an ancient wind pattern, which could be used to reconstruct the climatic record of a region. For example, Lancaster et al. (2002) used MGBNT on compound longitudinal dunes in Mauritania, demonstrating that three periods of dune construction in the past 25 ky coincided with distinct wind regimes.

We describe the rule of MGBNT and IMGBNT in detail below. The technique is then applied to aerial imagery of the Great Sand Dunes National Park and Preserve (GSDNPP) in Colorado, USA. Three different anemometers located near the dune field have obtained multiple-year wind measurements. These data indicate a wind regime consistent with that predicted by IMGBNT analysis, validating our technique.

2. Method

2.1. The rule of maximum gross bedform-normal transport

Experimental studies have shown that the orientation of a bedform is aligned as transverse as possible to all incident, sediment-bearing flows (Rubin and Hunter, 1987; Rubin and Ikeda, 1990). Mathematically, the gross bedform-normal transport $\boldsymbol{T}$ in any direction across a bedform trend can be represented as the sum of N transport vectors $\boldsymbol{Q_i}$ (e.g., measured sand fluxes) projected onto the gross bedform-normal transport:

$$\boldsymbol{T} = \sum_{i=1}^{N} \boldsymbol{Q_i} |\sin \alpha_i| \quad (1)$$

where α_i is the angle between each transport vector $\boldsymbol{Q_i}$ and the bedform trend. The bedform will develop so that it is aligned orthogonal to the maximum gross bedform-normal transport $\boldsymbol{T_m}$:

$$\boldsymbol{T_m} = \max \left(\sum_{i=1}^{N} \boldsymbol{Q_i} |\sin \alpha_i| \right) \quad (2)$$

In the most simple case, a unidirectional transport vector can be represented by a single vector $\boldsymbol{Q}$, producing the maximum gross bedform-normal transport $\boldsymbol{T_m}$ orthogonal to $\boldsymbol{Q}$: in other words, a pure transverse dune. Fig. 1 shows an example with two transport vectors, $\boldsymbol{Q}_1$ and $\boldsymbol{Q}_2$. The maximum gross bedform-normal transport (MGBNT) $\boldsymbol{T_m}$ represents all sand transport normal to the resulting bedform trend. In the case of two major sand-bearing winds, dune type and alignment is determined by only two parameters: the *transport ratio* ($|\boldsymbol{Q}_1|/|\boldsymbol{Q}_2|$) and the divergence angle ($\alpha_1 + \alpha_2$). Eq. (1) generalizes the case to any number of transport vectors.

The bedform trend is distinct from the resultant drift direction (i.e., RDD, the vector sum of all transport vectors $\boldsymbol{Q_i}$, shown as a green[1] arrow in Fig. 1), which may be orthogonal, parallel or oblique to the bedform trend (resulting in transverse, longitudinal, or oblique dunes, respectively). In conditions in which the direction and relative strengths of incident sand-bearing winds are known, the rule of MGBNT allows prediction of bedform type and orientation.

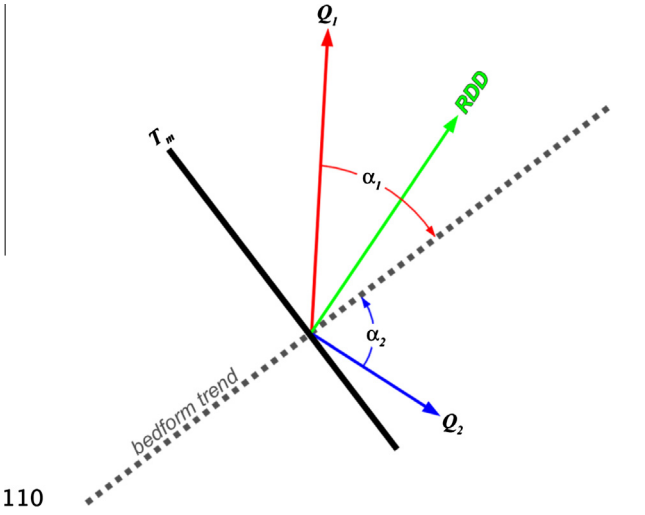

Fig. 1. The relationship between bedform trend and two incident sand-moving winds with transport vectors $\boldsymbol{Q}_1$ and $\boldsymbol{Q}_2$ as defined by Rubin and Hunter (1987). The resulting bedform trend is orthogonal to the gross bedform-normal transport $\boldsymbol{T_m}$. The angle between the resultant drift direction (RDD, the vector sum of transport vectors) and the bedform trend defines the bedform type (0–15° = longitudinal, 15–75° = oblique, 75–90° = transverse) as defined by Hunter et al. (1983).

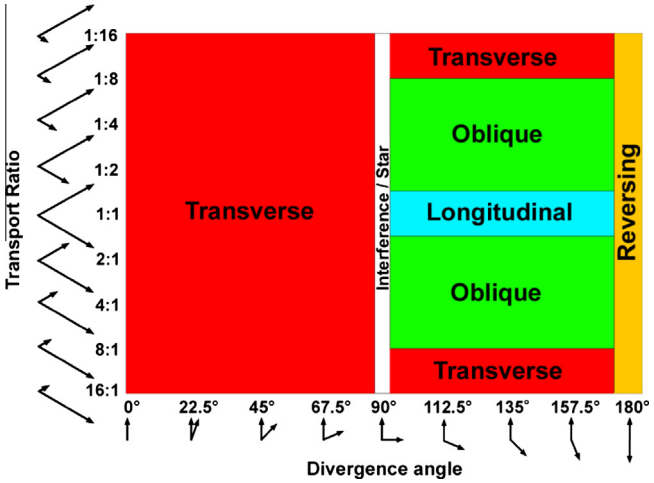

Fig. 2. Bedform types produced in a bimodal wind regime, as a function of the transport ratio $|\boldsymbol{Q}_1|/|\boldsymbol{Q}_2|$ and divergence angle $\alpha_1 + \alpha_2$. Dune classification mainly follows that determined experimentally by Rubin and Ikeda (1990) and Kocurek and Ewing (2005), with the addition of reversing dunes where winds are within 10° of directly opposing one another.

Fig. 2 shows the resulting bedform types produced by two sand-transporting winds, with transport ratios ranging from 1:16 to 16:1 and divergence angles 0–180° (based on Rubin and Ikeda, 1990; Kocurek and Ewing, 2005). Bedforms are considered to be transverse if the divergence angle is less than 90°, regardless of the transport ratio. They also form where the transport ratio is less than 1:8 or greater than 8:1; in these cases only the dominant wind strongly influences dune morphology, as though the dunes formed in a nearly unidirectional wind regime. Longitudinal dunes form only where the divergence angle is greater than 90° and the

[1] For interpretation of color in Figs. 1 and 3, the reader is referred to the web version of this article.

Please cite this article in press as: Fenton, L.K., et al. Inverse maximum gross bedform-normal transport 1: How to determine a dune-constructing wind regime using only imagery. Icarus (2013), http://dx.doi.org/10.1016/j.icarus.2013.04.001

two incident winds transport nearly the same amount of sand. Oblique dunes form where the divergence angle is greater than 90° and the two incident winds transport differing amounts of sand, with ratios ranging from 1:2–1:8 or 2:1–8:1. A transition occurs near a divergence angle of 90°, producing "interference dunes" with a transport ratio near 1:1 (e.g., Rubin and Ikeda, 1990; Dalrymple and Rhodes, 1995; Werner and Kocurek, 1997; Reffet et al., 2010; Rubin, 2012). These interference dunes are the same "dune networks" studied by Warren and Kay (1987) and Si (2002). Kocurek and Ewing (2005) label this range of divergence angles with star dunes. Although in nature star dunes are typically found in wind regimes with more than two major dune-building winds (e.g., Lancaster, 1989b), the overlapping crestlines produced by winds in this transition zone may be considered star dunes. We have added a fifth classification, that of reversing dunes, here defined as dunes formed in a bidirectional wind regime with any transport ratio, such that the two sand-bearing winds are separated by >170°.

2.2. Inverse maximum bedform-normal transport

With the rule of MGBNT, a bedform trend can be predicted with knowledge of the local sand-transporting winds. However, there are few locations beyond Earth where the wind regime is known with enough accuracy to predict the local bedform morphology. More typically, the known quantity is simply the bedform trend (and therefore, $\boldsymbol{T_m}$). With this information alone, the range of possible solutions to Eq. (2) is infinite. However, features created in unambigiously unidirectional wind regimes, such as yardangs, barchans, and wind streaks, are commonly located upwind of dune fields. If such features are present, it is often possible to make inferences about the direction of at least one transport vector (e.g., α_1).

By assuming that the wind capable of creating these unidirectional features (e.g., $\boldsymbol{Q}_1$) is at least partly responsible for dune construction, the concept of MGBNT can be inverted (IMGBNT). The result is a range of solutions consisting of possible sand-transporting winds (direction, transport ratio relative to $\boldsymbol{Q}_1$, and the resulting bedform type) that can combine with $\boldsymbol{Q}_1$ to produce the observed bedform trend (i.e., crestline set). Depending on "common sense" inferences regarding dune morphology, the resulting solution set may be further constrained. For example, if the bedforms being analyzed have broad, low-angle stoss slopes and steep slip faces that consistently face the same direction, it is then unlikely that such dunes are longitudinal.

While potentially of great use, the method outlined above has a few limitations. The first limitation is that only two incident winds may be determined at a time (i.e., $\boldsymbol{Q}_1$ and a range of solutions for $\boldsymbol{Q}_2$), whereas many dune fields are constructed under a multimodal wind regime, with winds varying in relative strength across the dune field. However, it is possible to step through a dune field, solving for new transport vectors (e.g., $\boldsymbol{Q}_3, \boldsymbol{Q}_4, \ldots$) that may combine with previously-determined transport vectors (e.g., $\boldsymbol{Q}_1$ and $\boldsymbol{Q}_2$) to produce different sets of bedforms.

Other limitations of this method restrict possible applications and place constraints on the interpretation of results. For example, the inferred initial transport vector orientation α_1 may be statistically derived from measurements (e.g., the mean of several yardang orientations), but at present it is represented by a single number. In reality, the dune-building wind directions may vary by several tens of degrees, over a period of time or across the dune field (or both). Another limitation is the necessary assumption of an initial transport vector direction, which may prove difficult to identify or ascertain. As with any model, the results are constrained by the quality of its inherent assumptions.

2.3. Procedure

Many dune fields consist of a complex array of superimposed dunes, with each group of distinctly-oriented and distinctly-sized crestlines representing a single generation of dune construction (Lancaster, 1999; Kocurek and Ewing, 2005). Furthermore, differently-oriented crestline segments on a single dune respond to an incident wind in a manner depending on the angle between the wind and each crestline segment (e.g., Hunter et al., 1983; Tsoar, 1983); notably, this appears to apply to star dunes as well (e.g., Nielson and Kocurek, 1987; Lancaster, 1989b; Zhang et al., 2000; Zhang et al., 2012). In other words, each dune segment (e.g., the arm of a star dune) may be regarded as transverse, oblique, or longitudinal to incident sand-moving winds, subject to the rule of MGBNT.

We apply these concepts to the Great Sand Dunes dune field. Beginning with 1-m digital orthophoto quarter quadrangles from the U.S. Natural Resources Conservation Service, the crestlines were mapped as polyline shapefiles in ArcGIS at a resolution of 1:4000. The crestlines were then grouped into eight sets based on similarity of morphology and orientation. Each different set of crestlines is assumed to represent a single bedform trend, type, and generation, such that it can be analyzed independently of neighboring crestlines.

Beginning with at least one observed set of unidirectional wind markers in the vicinity of the dune field (an inferred wind), the main crestline set was tested to determine what range of transport vectors would combine with the inferred wind to form the range (mean ± standard deviation) of observed crestline orientations. The solution set exists within a parameter space consisting of transport directions (0–360°), nine transport ratios relative to the known wind (1:16, 1:8, 1:4, 1:2, 1:1, 2:1, 4:1, 8:1, and 16:1), and bedform type (transverse, oblique, longitudinal, and reversing). If the resulting solution set is broad, then, if possible, it is refined based on inferences regarding dune morphology and the direction of net transport. The resulting constrained solution set may provide enough information to interpret the morphology and wind regime responsible for other crestline sets observed in the dune field.

2.4. Meteorology station data

Three meteorology (met) stations have collected data in the vicinity of the Great Sand Dunes for several years within the past decade, providing a detailed record of the wind regime at these locations. Their locations are indicated by magenta points in Fig. 3. The first met station was located at the GSDNPP Visitor Center, and recorded data at 10 min intervals from July 2002 through December 2004. The sand rose, resultant drift direction, and ratio of resultant drift potential to drift potential (RDP/DP) derived from these data were reported in Marín et al. (2005). The second met station is the Great Sand Dunes Remote Automated Weather Station (RAWS), which began operation in July 2004. Hourly wind data binned into 16 compass directions are freely available at http://www.raws.dri.edu/. Finally, the National Water Information System (NWIS) meteorology station has recorded atmospheric wind data with an ultrasonic sensor every 15 min since May 2009 at Indian Springs (site 374557105372401), with data freely available at http://waterdata.usgs.gov/nwis.

Using the method of Fryberger and Dean (1979), sand roses were constructed and the RDP/DP and RDD were estimated using meteorological data. With NWIS met station data, local air temperatures and pressures were used to calculate the local air density, allowing for estimates of potential sand drift. However, local air pressure measurements were not available for the RAWS site. With these data, local air temperatures were combined with the hydrostatic air pressure at the elevation of the met station to derive approximate local air density. Although this method does not

Please cite this article in press as: Fenton, L.K., et al. Inverse maximum gross bedform-normal transport 1: How to determine a dune-constructing wind regime using only imagery. Icarus (2013), http://dx.doi.org/10.1016/j.icarus.2013.04.001

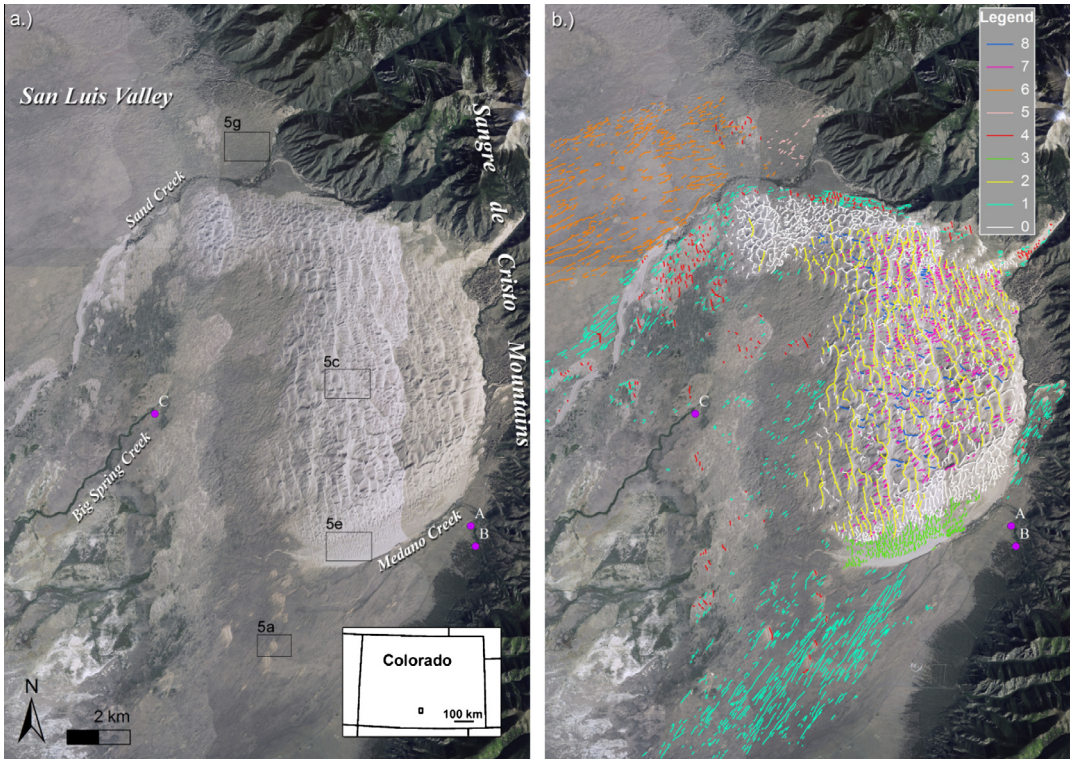

Fig. 3. The Great Sand Dunes in Colorado, USA (a) 1-m digital orthophoto quarter quadrangle from the U.S. Natural Resources Conservation Service, showing the locations of three meteorology stations (A = The GSDNPP Visitor Center, B = RAWS, C = NWIS Indian Springs met station), boxes indicate the locations of subfigures in Fig. 5, (b) the same scene showing mapped crestlines, including eight identified sets as well as those left uncategorized (white).

account for pressure fluctuations driven by weather systems, it does provide a first-order estimate of the sand-moving capacity of winds near the weather station.

Sand drift potentials are also used to estimate the resulting bedform trend using MGBNT. The expected bedform type is determined by the smallest angle between the RDD and the bedform trend; following Hunter et al. (1983), bedform trends less than 15° from the RDD are considered longitudinal, greater than 75° are considered transverse, and 15–75° are considered oblique.

3. The Great Sand Dunes of Colorado, USA

3.1. Dune morphology

3.1.1. Overview

The Great Sand Dunes are located in the Great Sand Dunes National Park and Preserve within the eastern San Luis Valley of Colorado, USA, along the western front of the Sangre de Cristo Mountains (see Fig. 3). The main dune field (37°47′N, 105°33′W) encompasses ~72 km^2, but aeolian sand sheets and low-relief, mostly vegetated dunes cover a further ~553 km^2 of terrain to the southwest, west, and northwest of the main dune field (Madole et al., 2008). Aeolian sediment is mainly derived from the "sump", a closed basin consisting of dry lakebeds on the floor of the San Luis Valley (Madole et al., 2008). This sand is blown northeastward by prevailing winds, forming parabolic dunes, blowouts, and low-lying dunes, until it meets opposing winds blowing down the slope of the Sangre de Cristo range (e.g., Valdez et al., 2007). The tallest dunes of the Great Sand Dunes have formed where these air flows collide. Madole et al. (2008) proposed that the dune field began accumulating before ~130 ka. Optically stimulated luminescence (OSL) dating revealed that five periods of significant aeolian deposition have occurred on the sand sheets in the San Luis Valley in the past 700 years, indicating that influx of sand into the main dune field is episodic (Forman et al., 2006). The mean annual precipitation in the GSDNPP is 28.17 ± 7.90 cm/yr, wetter than that where desert dunes typically form (A. Valdez, personal communication, 2013).

The Great Sand Dunes were chosen as a suitable location for testing the IMGBNT method for a number of reasons. The dunes are not easy to understand upon inspection, providing an interesting challenge. Their morphology has not yet been studied in detail, making them an "unsolved problem". Three meteorology stations adjacent to the main dune field have accumulated years of wind data, making spatial variations in the wind regime easier to identify (an uncommon luxury). Finally, the Great Sand Dunes are a good analog for many martian dune fields, which are similarly located near steep topography and are thus subject to both regional and local terrain-influenced air flows (e.g., Silvestro et al., 2012). This technique has potential applications in planetary aeolian environments, in which high resolution imagery is plentiful but wind measurements are scarce.

The dunes of the GSDNPP show a variety of aeolian morphologies, many of which are not well studied. The vegetated dunes upwind of the main dune field are predominantly parabolic dunes, with arms aligned with the resultant drift direction calculated from wind measurements made at the Visitor Center of the Great Sand Dunes National Park and Preserve (Fig. 4a; Marín et al., 2005). Migration rates of ~8 m/year have been measured on these dunes using imagery from the early through late 20th century, with episodes of dramatic acceleration corresponding to dry periods in the precipitation record (Marín et al., 2005).

The main dune field displays far more intricate morphologies than dunes on the surrounding sand sheets. Dominant north–south trending dunes have been described as transverse, although they occasionally develop reversing slip faces (see references within

Please cite this article in press as: Fenton, L.K., et al. Inverse maximum gross bedform-normal transport 1: How to determine a dune-constructing wind regime using only imagery. Icarus (2013), http://dx.doi.org/10.1016/j.icarus.2013.04.001

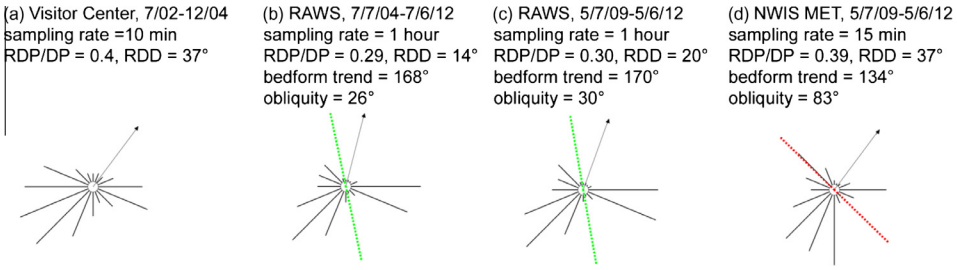

Fig. 4. Sand roses, operational time periods, sampling rate, and associated calculations for each of the three meteorology stations near the Great Sand Dunes (for locations see A, B, and C in Fig. 3). (a) Met station data at the GSDNPP Visitor Center, with results reported by Marín et al. (2005), (b) RAWS over an 8 year time period, (c) RAWS over a 3 year time period coincident with (d) NWIS met station. Arrows represent RDD; colored lines represent orientation and type of dune predicted by MGBNT using the measured wind regime (red where the angle between dune orientation and RDD, the dune obliquity, is 75–90° and green where this angle is 15–75°). (For interpretation of the references to color in this figure legend, the reader is referred to the web version of this article.)

Madole et al. (2008)). Madole et al. (2008) also identified a second, less clearly visible set of transverse dunes trending northwest-southeast in the east-central part of the main dune field. Valdez et al. (2007) described the main dune field as a complex draa with five depocenters that are each considered to be individual draa. They report that reversing and star dunes dominate the dune morphology, with smaller dome, barchan, barchanoid, transverse, and reversing dunes forming on the margins. The southern edge of the main dune field is delineated by Medano Creek, which occasionally floods, eroding sand from the dunes (Fryberger, 1999). Dunes bordering Medano Creek are smaller than those in the rest of the main dune field, although their crestlines are similarly aligned to the large north–south reversing dunes. Flooding in the creek may periodically destroy these smaller dunes, which then begin to rebuild as younger versions of the large dunes that dominate the dune field. This idea is consistent with their young age (<300 years, Valdez et al., 2007).

Mapped crestlines were categorized into eight sets based on dune size, orientation, and morphology; each of these sets is described in detail below. Some crestlines were difficult to place into a category, either because they appeared to match criteria for more than one set or because they did not match criteria for any set; these crestlines remained uncategorized and are shown in white in Fig. 3b. Such crestlines are most common at the northern and southern edges of the main dune field, reflecting an intricate wind regime and sedimentary history. The northern fifth of the dune field consists of two draa (the Cold Creek and Sand Creek draa of Valdez et al., 2007) that are dominated by star dunes and parabolic dunes that wrap around the northern edge of the dune field, indicating that this is a region with a multimodal, spatially shifting wind regime. Near the southern edge of the dune field, dune morphology is difficult to interpret where small dunes (see Section 3.1.4) appear to transition to the larger dunes that comprise the main portion of the dune field. The following sections describe each crestline set in more detail.

3.1.2. Set 1: Parabolic dunes

The first set of crestlines (Set 1, in cyan in Fig. 3b) consists of the more prominent arms of parabolic dunes on sand sheets surrounding the main dune field. Most of these dunes lie upwind (southwest) of the main dune field (Fig. 5a and b), but some can also be found to the north and southeast of the main dune field. Valdez (2012) describes an "escape dune", an example of one of these dunes found immediately southeast of the main dune field, riding up against the Sangre de Cristo range. It has migrated towards the northeast at 8.6 m/year, a rate similar to other parabolic dunes southwest of the main dune field (Marín et al., 2005). Collectively these dunes have a mean orientation and standard deviation of 44° ± 18° (Fig. 6a). However, some of these dunes wrap around the north edge of the main dune field, bending towards the east–southeast. Excluding these anomalous dunes, which are subject to local (probably topographic) influences on the wind, the remainder are more tightly grouped at 39° ± 10°. This orientation matches well with previous measurements, as well as their migration direction (Marín et al., 2005). Assuming that parabolic dune arms and migration directions are associated with a major sand-transporting wind in the region, we infer that wind blowing from ~219° clockwise from north (henceforth termed the *SW wind*) strongly influences the morphology of the Great Sand Dunes. It is remarkable that such consistent morphology and unidirectional migration can be found in vegetated dunes adjacent to the main dune field, where intricate and spatially-varying dune morphology reflects a multi-modal wind regime. Vegetation is one of several stabilizing agents that can force dunes to follow the RDD, rather than reflect the behavior of a potentially complex wind regime (e.g., Rubin and Hesp, 2009).

3.1.3. Set 2: Large north–south dunes

In Set 2 (in yellow on Figs. 3b and 5c) are the large north–south oriented dunes that dominate the morphology of the dune field. These dunes are among the easiest to identify as a result of their sharp crestlines, and have a mean orientation of 171° ± 19° (Fig. 6b). Madole et al. (2008) summarized previous descriptions of their morphology, with classifications ranging from barchanoid, transverse, to reversing. Steeper east-facing slopes are consistent with transverse, oblique, or reversing dunes with a dominant transport direction towards the east. Small reversing slip faces that occasionally form at the crests (visible in Fig. 5d) support at least a small amount of westward sand transport, although it is unclear how effectively this transport may have determined their current morphology and orientation. The crestlines are oriented oblique to the SW wind, suggesting that at least one other sand-transporting wind strongly influences their bedform trend.

3.1.4. Set 3: Small north–south dunes

Set 3 covers a small area of transverse dunes at the southern edge of the main dune field (in green in Figs. 3b and 5e). These dunes are roughly parallel to the main reversing dunes, with a mean orientation of 179° ± 17°. In Fig. 5e they appear to be transverse to an easterly wind, with steeper slopes on their western sides. However, these dunes change on a decadal timescale (see Fig. 3 of Forman et al. (2006)), and they are located in a region of actively forming dunes. Because of their similar orientation relative to the larger dunes of Set 2, it is likely that these dunes are a smaller, younger version of the same dunes that ultimately developed into the grand dunes of Set 2. As with the Set 2 crestlines, these dunes are aligned oblique to the SW winds and contain shorter (unmapped) crest elements in a different orientation altogether

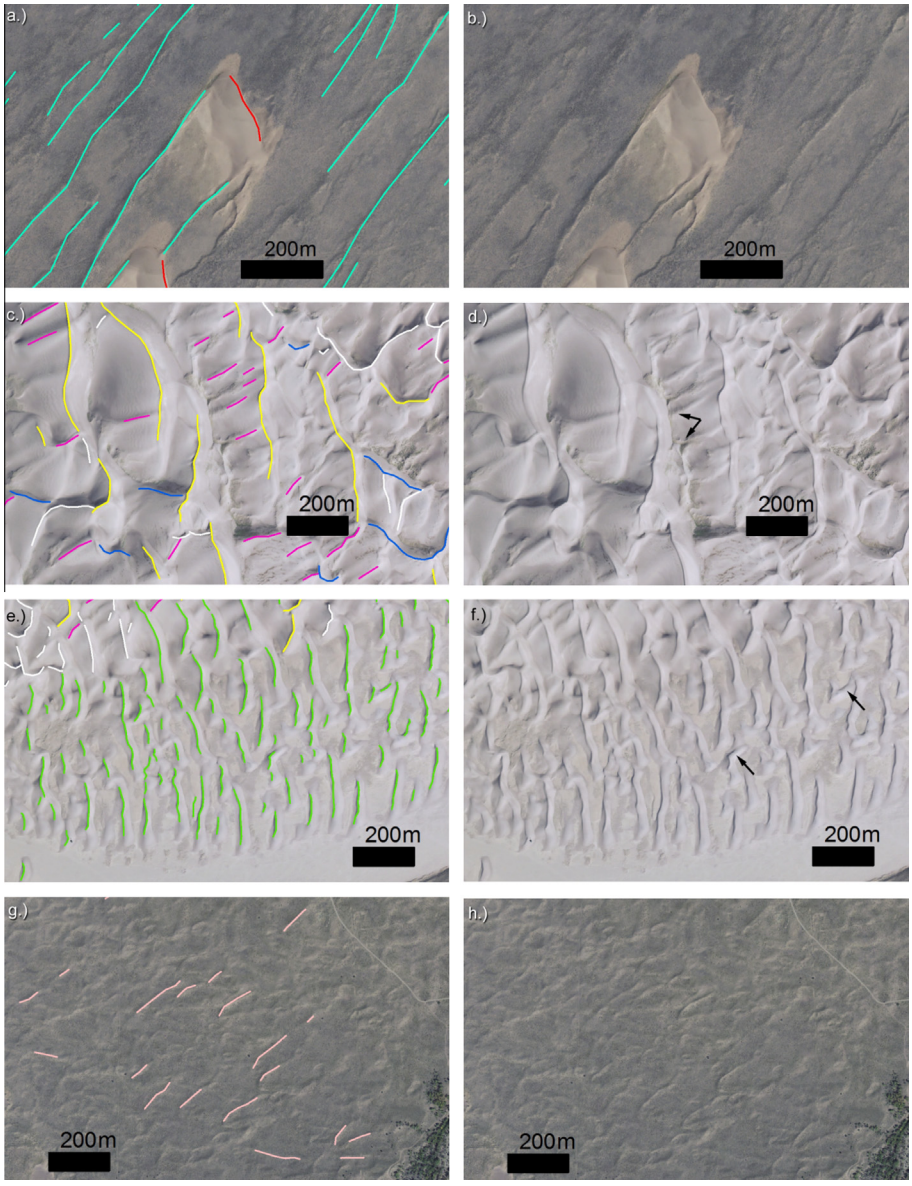

Fig. 5. Examples of dunes in the GSDNPP, with locations shown in Fig. 3. (a and b) Parabolic dunes (Set 1, cyan) and their active transverse elements (Set 4, red). (c and d) Large north–south aligned crests (Set 2, yellow), short linear crestlines (Set 7, magenta), NW–SE aligned crests (Set 8, blue), and unclassified crestlines (white) in the main dune field. (e and f) Small north–south aligned crests (Set 3, green) at the southern edge of the main dune field. (g and h) Southwest-trending parabolic dunes north of the main dune field (Set 5, pink). (For interpretation of the references to color in this figure legend, the reader is referred to the web version of this article.)

(see arrows in Fig. 5e). These factors suggest that the incident dune-building winds may be more complex than those that create pure transverse or reversing dunes.

3.1.5. Set 4: Active elements of parabolic dunes

Set 4 (in red in Figs. 3b and 5a), consists of transverse elements of parabolic dunes on the sand sheet upwind of the main dune field (see Fig. 3). In other dune fields, parabolic dunes typically end in a rounded nose on their downwind edges. More active parts of such dunes, typically near the nose, can form into barchanoid dunes with crestlines aligned normal to the parabolic arms. Both types of dunes reflect one major sand-transporting wind. However, the active elements of these parabolic dunes are on average oriented ~30° clockwise from a line orthogonal to the SW wind. These rotated crestlines require at least one other major sand-transporting wind to form, to prevent them from forming transverse to the SW wind that appears to control the parabolic dune arms. The juxtaposition of the Set 4 dune elements on the Set 1 parabolic dunes supports the proposal by Rubin and Hesp (2009) that vegetation can force dunes to align with the RDD. Furthermore, the prevalence of these angled crestlines throughout the sand sheet suggests that a multidirectional wind regime spans the region surrounding the dune field.

3.1.6. Set 5: Parabolic dunes north of the main dune field

North of the main dune field and north of Sand Creek is a small area just west of the Sangre de Cristo Mountains that is covered by a sand sheet with a complex pattern of crestlines. The more prominent crestlines (Set 5, in pink in Figs. 5g and 6e) appear to be formed by parabolic dunes migrating towards the southwest, away from the reentrant in the mountain range from which Sand Creek emerges. There is no other direct evidence for a northeasterly wind in this area, and it is unclear how much sand transport occurs due to this wind.

Please cite this article in press as: Fenton, L.K., et al. Inverse maximum gross bedform-normal transport 1: How to determine a dune-constructing wind regime using only imagery. Icarus (2013), http://dx.doi.org/10.1016/j.icarus.2013.04.001

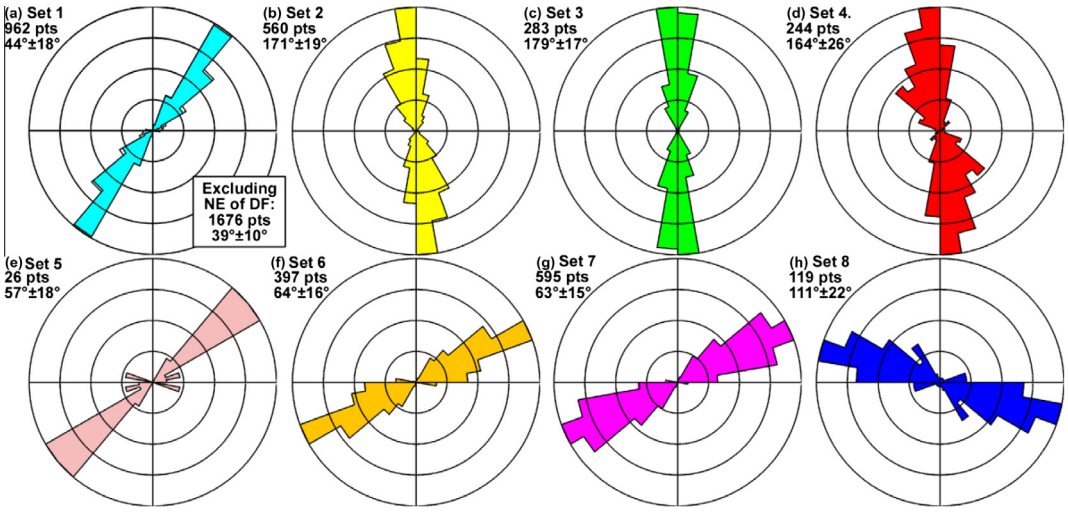

Fig. 6. Normalized polar histograms of mean dune crestline orientations in the Great Sand Dunes. Colors correspond to crestline sets shown in Fig. 3b and Fig. 5. Mean orientations given in degrees between 0° and 180°; the histograms are mirrored for viewing ease. Note that (a) shows two distributions, with the more saturated histogram corresponding to crestlines that do not include those north and east of the main dune field. (For interpretation of the references to color in this figure legend, the reader is referred to the web version of this article.)

3.1.7. Set 6: Parabolic dunes NW of the main dune field

North and west of the main dune field, across Sand Creek, is Set 6 (in orange on Figs. 3b and 6f) parabolic dunes that are similar in morphology to the Set 1 parabolic dunes. They are mostly stabilized, with a few active crests categorized in Set 4. More notably, their orientation is 64° ± 16°, ~25° clockwise of the Set 1 crestlines. The shift in bedform trend may reflect either a temporal or spatial shift in wind regime, and it may contribute (along with the northeasterly wind responsible for Set 5) to the increased complexity in the Cold Creek and Sand Creek draa at the northern edge of the main dune field.

3.1.8. Set 7: Short, linear crestlines in the main dune field

Magenta crestlines shown in Figs. 5c and 6g correspond to Set 7, a group of dunes 50–100 meters long, located mainly on the western flanks of the large north–south oriented dunes. These features span the same area covered by the larger dunes, and they often extend from vegetated structures that, based on erosional features and steep slopes, appear to be more competent than typical dune sand (see black arrows in Fig. 5d). These structures appear similar to the edges of blowouts and parabolic dunes found southwest of the main dune field, and on the western edge of the dune field, one appears to grade into the other. Care was taken to mark only the trend of the crestlines free of this more cohesive material, to ensure that only the free bedform trend is represented (although qualitatively, the cohesive and noncohesive aspects of these bedforms are similarly oriented). It is not clear from their morphology what sort of bedform they may be: they do not present any slip faces and their lateral sides appear roughly symmetrical, such that any transverse component to their migration is not easily discerned from imagery alone.

These bedforms may be lee dunes formed by a southwest wind. However, they are oriented ~19° clockwise relative to the parabolic dunes of Set 1. This rotation may reflect a corresponding shift in the wind pattern, perhaps forced by proximity to the Sangre de Cristo mountains. Alternatively, these dunes may be superimposed bedforms, which formed within a boundary layer shaped by the topography of larger dunes of Set 2 beneath them. If this is the case then the Set 7 dunes experience a wind regime modified from the regional winds that produce the main crestlines of Set 1. However, it is probable that, like the parabolic dunes of Set 1, the Set 7 dunes are most strongly influenced by a wind with a strong southwesterly component.

3.1.9. Set 8: NW–SE crestlines in the main dune field

The final crestline set (blue in Figs. 5c and 6h) corresponds to northwest–southeast trending dunes that appear to have slip faces on their northeast faces, such that they are oriented mainly transverse to a southwesterly wind. These are the same as "T/R2" dunes discussed by Madole et al. (2008), although they do not appear as prominently in Fig. 3 as in the Landsat image from their paper. Of all crestlines, these were the most difficult to clearly identify, and it is possible that they are extensions of the large yellow crestlines of Set 2. Assuming they stand alone as a distinct set of dunes, they are slightly oblique to the SW wind, with a mean angular separation of 72°. Together, the combined Set 2 and Set 8 crestlines have a mean and standard deviation orientation of 163° ± 30°, which is also oblique to the SW wind.

3.2. Analysis of the Great Sand Dunes

3.2.1. IMGBNT analysis of the Set 2 crestlines

Determining the wind regime that produced the Set 2 crestlines requires use of IMGBNT, with the known and inferred quantities being the bedform trend and SW wind, respectively. The unknown quantity is the range of wind directions that can combine with the SW wind to produce the observed bedform trend. Fig. 7 shows the SW wind (219°) and the mean crestline orientation in black. Shaded regions correspond to possible solutions of IMGBNT (orientation corresponds to wind direction, magnitude corresponds to the transport ratio, and colors correspond to the resulting dune type).

A brief inspection shows that winds with either strong easterly or strong westerly components are required to create the observed dunes. Winds ranging from WSW to NW would combine with the 219° wind to produce eastward-migrating transverse dunes. Winds ranging from ENE to SE would combine with the 219° wind to produce a variety of morphologies, depending on their strength relative to the SW wind.

It is possible to constrain the solution further by making inferences regarding the dune morphology. East-facing slopes are shorter and steeper (see Fig. 5c and d), as would be the case if they were

Please cite this article in press as: Fenton, L.K., et al. Inverse maximum gross bedform-normal transport 1: How to determine a dune-constructing wind regime using only imagery. Icarus (2013), http://dx.doi.org/10.1016/j.icarus.2013.04.001

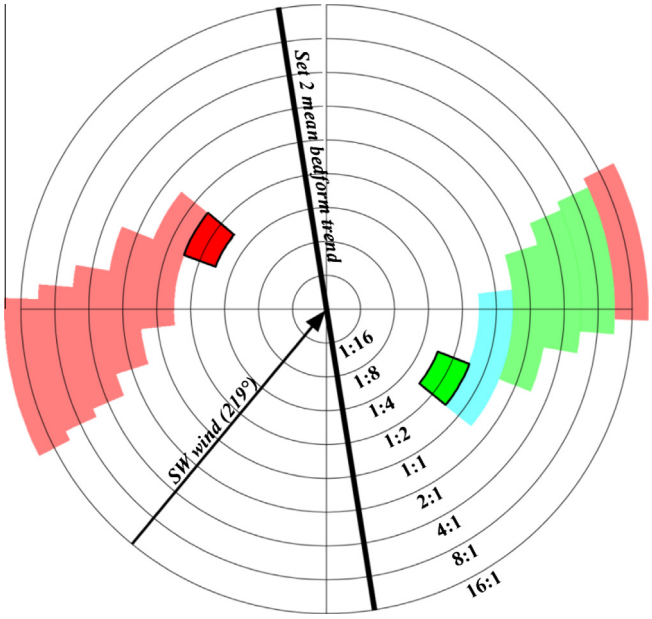

Fig. 7. Plot of incident transport vectors that could combine with the SW wind (from 219°) to produce the observed bedform trend of Set 2, the yellow crestlines. Each circle corresponds to a transport ratio relative to the SW wind (e.g., 1:2 indicates a non-SW wind with a transport magnitude half that of the SW wind). Colors correspond to resulting bedform type (red = transverse, green = oblique, cyan = longitudinal). The most probable results are highlighted and outlined in black, suggesting that the large dunes of the main dune field are either transverse or oblique, or some combination. Prominent reversing slip faces on the western slopes indicate that wind with an easterly component modifies the dunes, making the subset of oblique solutions more likely. (For interpretation of the references to color in this figure legend, the reader is referred to the web version of this article.)

the main slip faces. In addition, the lower portion of the dunes are dominated by crossbedding deposited by southwesterly winds (Merk, 1960). Therefore it appears likely that the SW wind has a greater influence on the development of these dunes than any other sand-transporting winds. By restricting the solution to those in which the SW wind dominates (a transport ratio from 1:1 to 16:1), the range of likely sand-transporting winds narrows considerably. Fig. 7 shows these remaining winds outlined in black: either a northwesterly wind (291–309°) produces transverse dunes with a NW:SW transport ratio of 1:2, or a southeasterly wind (111–129°) produces oblique dunes with a SE:SW transport ratio of 1:2. The observation of small, west-facing reversing slip faces on these dunes suggests that wind with an easterly component plays a role in shaping the dunes; therefore we propose that the large crests of the main dune field are oblique to SW and SE winds, with SW winds dominating sand transport by approximately a factor of two.

There is no direct evidence that a northwesterly wind influences the morphology of these dunes, bringing the 291–309° wind into question. However, the abundance of star dunes (e.g., Valdez et al., 2007) implies that more than two main winds have helped to construct the dune field. Furthermore, the combination of SW and SE winds would lead to nearly northward transport: the resultant potential sand drift of a SE wind (111–129°) and a SW wind (219°) in a 1:2 ratio is 10–12°. This would lead to the dune field extending northward across the Sangre de Cristo range, which has not happened. Rather, the areas where sand has migrated beyond the dune field extend northeast into re-entrants in the Sangre de Cristo range; further northeastward movement is impeded by Sand and Medano Creeks. A northwesterly wind would balance the SE flow, both reducing the net transport and maintaining a northeastward RDD.

It is likely that these narrow solutions to IMGBNT do not represent the full range of wind directions modifying the dune field. The parabolic dunes of Set 1 provide the rationale for the SW wind, but it is probably an oversimplification to represent it as a single wind blowing from 219°. Therefore the range of winds that may combine with the SW wind to produce the observed bedform trend is almost certainly broader than that shown in Fig. 7. As a result we describe these winds qualitatively as the *SE wind* and *NW wind*.

The crestlines of Set 3 have mean orientations similar to those of Set 2. As noted in Section 3.1.1, the dunes at the southeastern edge of the main dune field (Set 3) are periodically disrupted by floods in Medano Creek, and probably represent a smaller and younger version of the larger crests of Set 2. The similarity of these two sets of dunes suggests they reflect a similar wind regime, such that winds from the SE and SW with a 1:2 transport ratio strongly influence their morphology. The NW wind may be partially responsible for the short, unmapped elements of dunes that extend from these crests (arrows in Fig. 5e).

The crestlines of Set 4 are also aligned similarly to those of Set 2. IMGBNT analysis would produce a solution set similar to that of Fig. 7, indicating that the Set 4 crestlines are likely oblique to a SE and SW wind with a 1:2 transport ratio (respectively). The area spanned by these crestlines extends far beyond the main dune field, suggesting that the SW and SE (and possibly the NW) winds impact a broad area of the eastern San Luis Valley.

The results of IMGBNT analysis can also be applied to crestline Sets 7 and 8. Given the evidence for a substantial transport vector from the southwest, it seems likely that the crestlines of Set 7 formed due to SW winds as lee dunes on the stoss slopes of the large north–south dunes (Set 2 crests). Southeasterly and northwesterly winds may modify these crests, in the same way that secondary flows help to form and maintain star dune arms (e.g., Lancaster, 1989a), but without further data the influence of these winds cannot be determined. The Set 8 crestlines may not represent a fully distinct category of crestlines, but rather a subset of the Set 2 crestlines. They may indicate that the SW wind is not well described by a single direction, but instead should be regarded as a wider distribution of winds; for example, the Set 8 crestlines could be transverse elements of large dunes that respond to a SSW wind.

3.2.2. Comparison with meteorology station data

Fig. 4 shows the sand roses and lists the RDD and RDP/DP derived from the three meteorology stations located near the main dune field (see Fig. 3, Section 3.1.1). There is very little overlap in time between the Visitor Center met station and the RAWS, so there may be interannual differences in sand transport that complicate the interpretation of the data. However, there is a full 3 year overlap between the RAWS and the NWIS data; Fig. 4c shows a subset of the 8 year RAWS data set that coincides with NWIS data (shown in Fig. 4d). Results from the 3 and 8 year RAWS data sets are similar enough to suggest that a 3 year baseline characterizes the range of sand-moving winds at the Great Sand Dunes.

All three sensor sites indicate that southwesterly winds dominate the local sand transport, with a resultant drift direction towards the NNE to NE. All three sites also indicate significant drift potential by winds from the east to SE as well as winds from the west to NW. These results are consistent with that predicted by IMBGNT analysis of the long Set 2 crestlines in the main dune field (compare with Fig. 7). MGBNT analysis of the RAWS data produces an oblique bedform oriented to 168° (Fig. 4b), which compares favorably with the orientations of the crestlines of Sets 2–4 (as well as the combined Sets 2 and 8). Thus, the IMGBNT analysis presented in Section 3.2.1 is consistent with the known wind regime. Furthermore, the inferences required for IMGBNT analysis appear to be robust: the parabolic dune arms of Set 1 are aligned with

Please cite this article in press as: Fenton, L.K., et al. Inverse maximum gross bedform-normal transport 1: How to determine a dune-constructing wind regime using only imagery. Icarus (2013), http://dx.doi.org/10.1016/j.icarus.2013.04.001

the SW wind, and the large Set 2 crestlines are also dominated (but not wholly formed) by the SW wind.

MGBNT analysis of the 3-year NWIS data predicts a bedform trend of 134°, nearly orthogonal to the RDD of 37°. This is consistent with the nearby Set 1 parabolic dune arms, which are aligned nearly parallel to the RDD. However, the result is not consistent with the Set 4 transverse elements of the parabolic dunes (see Fig. 6d), which are aligned 30° counter-clockwise to the predicted bedform trend. It is not clear why the NWIS data does not indicate an oblique wind regime, as expected from the Set 4 crestlines. It is possible that the location of the Indian Springs met station near the bank of Big Spring Creek may affect the measured local wind pattern. The topographic channel formed by the southwestward-flowing creek may concentrate southwesterly winds, enhancing their sand transport relative to other winds in the immediate vicinity of the creek. Thus the met station may record a more predominantly unidirectional wind regime than is found on the sand sheet nearby (the nearest Set 4 crestlines are ~500 m to the north, and are likely unaffected by any local influence of the Big Spring Creek).

4. Discussion

All met stations indicate that the SW wind varies in direction to some degree, although our analysis assumed that a uniform wind from 219° was the only wind from the SW. The spread in incident SW winds is likely reflected by a corresponding spread in crestline orientations (standard deviations range from ±15° to 26°). The parabolic dunes are aligned more consistently than the measured range of SW winds (the standard deviation of the bulk of Set 1 is ±10°). The straightness of the parabolic dune arms indicates that the wind regime has not undergone a significant shift during their period of formation. The tight grouping of orientations suggests that in a multimodal wind regime such as that experienced at the GSDNPP, parabolic dunes align to the RDD rather than simply to the strongest and most frequent sand-transporting wind.

Fig. 8 shows the gross bedform-normal transport (GBNT) from the 8-year RAWS data (green) and 3 year NWIS data (red). Plot maxima correspond to the direction of MGBNT (i.e., the predicted bedform trend), shown in Fig. 4b and d. Subtle inflection points in the RAWS GBNT are caused by the quantized nature of the wind directional data, which were recorded at 16 compass directions (the NWIS data have a directional resolution of one degree and suffer no such issues). Neither plot contains secondary maxima, indicating that the predicted bedform trend should be the only one present. However, this is not the case: MGBNT does not predict the presence of parabolic rather than transverse dunes on the sand sheet upwind of the main dune field, nor does it predict the presence of the Sets 7 and 8 crestlines.

These inconsistencies can be explained by a closer look at local conditions. A high precipitation rate within the sand sheet enhances vegetation growth; combined with a high migration rate, parabolic dunes form the Set 1 crestlines, rather than the transverse dunes predicted from MGBNT analysis (Barchyn and Hugenholtz, 2012). A similar effect may produce the cohesive structures observed on the western flanks of the large dunes of the main dune field (see arrows in Fig. 5d). In this case blowouts may begin to form when sand is saturated with ice or water, creating erosional features that later serve as obstacles for the formation of lee dunes (i.e., the Set 7 crestlines). Thus, the Set 1 and Set 7 dunes may be two different types (parabolic and lee dunes, respectively) of the class of longitudinal bedforms outlined by Rubin and Hesp (2009). In addition, the Set 7 (and possibly Set 8) dunes may be superimposed bedforms, subject to winds within the boundary layer formed by the larger dunes. The combination of their longitudinal nature and subjectivity to local boundary layer conditions likely explains why their orientations cannot be predicted from MGBNT analysis of wind data.

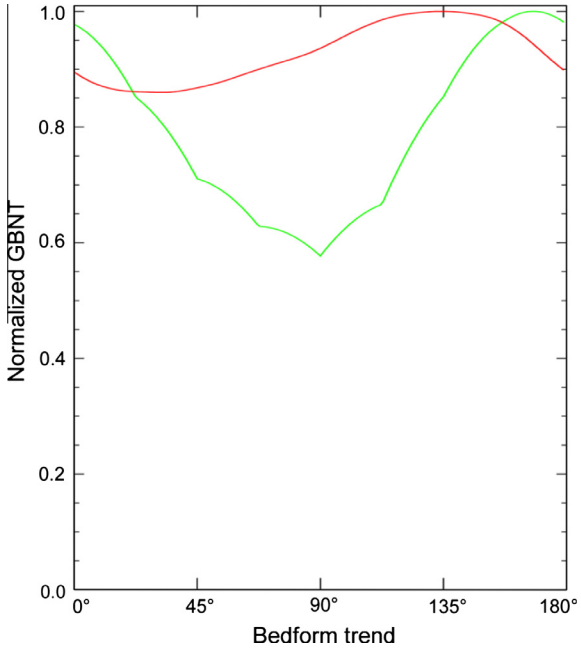

Fig. 8. Gross bedform-normal transport curves as a function of bedform trend, calculated from 8 years of RAWS data (green) and 3 years of NWIS data (red). Maxima are labeled in Fig. 4. Note that each curve has only one, broad maximum, indicating that only one type of dune is predicted to form at each station location. (For interpretation of the references to color in this figure legend, the reader is referred to the web version of this article.)

The single, well-defined, broad peak in the RAWS GBNT plot is inconsistent with the Set 8 crestlines. As suggested by morphology and IMGBNT, these crestlines are most likely part of a broad set of crestlines that encompasses both Sets 2 and 8. Their presence likely indicates complex wind direction variability in the three main sand-moving winds. If the Set 8 dunes are superimposed bedforms, then their nature cannot be understood from MGBNT analysis of regional wind patterns. Further study of flows within the boundary layers produced by large dunes are needed to unravel the relation between superimposed bedforms and their orientations.

5. Conclusions

We have developed a technique to determine the major sand-bearing winds incident on a dune field by inverting the rule of maximum gross bedform-normal transport. Although any number of winds can combine to produce a given crestline orientation, the possible solution set can be constrained by limiting the analysis to two winds at a time and making inferences about resultant drift directions and dune morphology.

The technique was applied to the Great Sand Dunes of Colorado, USA. Parabolic dune arms located southwest of the main dune field provided an inferred wind direction from the southwest. Possible winds that could combine with this southwesterly wind to produce long north–south trending crestlines in the main dune field can be constrained to southeasterly and northwesterly winds, each with a 1:2 transport ratio relative to the dominant southwesterly wind. Based on morphological observations, the southeasterly wind likely plays a more prominent role in shaping the dunes than the northwest wind. Other dune crestlines can be explained with these three winds, or do not impact the bulk of the main dune field. The resulting predicted wind regime compares favorably with that

Please cite this article in press as: Fenton, L.K., et al. Inverse maximum gross bedform-normal transport 1: How to determine a dune-constructing wind regime using only imagery. Icarus (2013), http://dx.doi.org/10.1016/j.icarus.2013.04.001

measured by three different meteorological stations, located adjacent to the main dune field, providing a validation of the method.

This technique has applications in areas where bedforms are present and the surface has been imaged at a high spatial resolution, but little or no meteorological data is available. Specifically, remote regions on Earth and nearly all planetary sites with observable bedforms are good candidates for using this method. In areas where the winds are measurable, this method could be used on stabilized dunes to infer ancient wind regimes (e.g., Lancaster et al., 2002). Used in concert with pattern analysis (e.g., Ewing et al., 2006), this method could be applied to quantify the boundary conditions that control the aeolian history of a dune field.

Acknowledgments

We thank Dave Rubin and Claire Newman for many helpful conversations that led to this work, and Simone Silvestro and David Vaz for help with ArcGIS. In addition we thank Dave Rubin and Andrew Valdez for reviews that improved and strengthened the manuscript. This work was conducted independent of grant support.

References

Barchyn, T.E., Hugenholtz, C.H., 2012. Predicting vegetation-stabilized dune field morphology. Geophys. Res. Lett. 39, L17403. http://dx.doi.org/10.1029/2012GL052905.

Chittenden, J., Chevrier, V., Roe, L., Bryson, K., Pilgrim, R., Sears, D., 2008. Experimental study of the effect of wind on the stability of water ice on Mars. Icarus 196, 477–487. http://dx.doi.org/10.1016/j.icarus.2008.01.016.

Dalrymple, R.W., Rhodes, R.N., 1995. Estuarine dunes and bars. In: Perillo, G.M.E. (Ed.), Geomorphology and Sedimentology of Estuaries: Developments in Sedimentology, vol. 53. Elsevier, pp. 359–422.

Elbelrhiti, H., Claudin, P., Andreotti, B., 2005. Field evidence for surface-wave-induced instability of sand dunes. Nature 437, 720–723. http://dx.doi.org/10.1038/nature04058.

Elbelrhiti, H., Andreotti, B., Claudin, P., 2008. Barchan dune corridors: Field characterization and investigation of control parameters. J. Geophys. Res. 113, F02S15. http://dx.doi.org/10.1029/2007JF000767.

Ewing, R.C., Kocurek, G., 2010a. Aeolian dune-field pattern boundary conditions. Geomorphology 114, 175–187. http://dx.doi.org/10.1016/j.geomorph.2009.06.015.

Ewing, R.C., Kocurek, G.A., 2010b. Aeolian dune interactions and dune-field pattern formation: White Sands Dune Field, New Mexico. Sedimentology 57, 1199–1219. http://dx.doi.org/10.1111/j.1365-3091.2009.01143.x.

Ewing, R.C., Kocurek, G., Lake, L.W., 2006. Pattern analysis of dune-field parameters. Earth Surface Process. Landforms 31, 1176–1191. http://dx.doi.org/10.1002/esp.1312.

Fenton, L.K., Bandfield, J.L., Ward, A.W., 2003. Aeolian processes in Proctor Crater on Mars: Sedimentary history as analyzed from multiple data sets. J. Geophys. Res. 108, E12, 5129, doi:10.1029/2002JE002015.

Forman, S.L. et al., 2006. Episodic Late Holocene dune movements on the sand-sheet area, Great Sand Dunes National Park and Preserve, San Luis Valley, Colorado, USA. Quaternary Res. 66, 97–108. http://dx.doi.org/10.1016/j.yqres.2005.12.003.

Fryberger, S.G., 1999. Overview of the eolian depositional system, Great Sand Dunes National Monument and vicinity. In: Schenk, C.J. (Ed.), Hydrologic, Geologic and Biologic Research at Great Sand Dunes National Monument, Colorado: Proceedings of the National Park Service Research Symposium, No. 1, USGS, Denver, CO, pp. 195–214.

Fryberger, S.G., Dean, G., 1979. Dune forms and wind regimes. In: McKee, E.D. (Ed.), A Study of Global Sand Seas. US Geological Survey Professional Paper 1052, pp. 137–140.

Hayward, R.K. et al., 2007. Mars Global Digital Dune Database and initial science results. J. Geophys. Res. 112, E11007. http://dx.doi.org/10.1029/2007JE002943.

Hisatake, K., Tanaka, S., Aizawa, Y., 1993. Evaporation rate of water in a vessel. J. Appl. Phys. 73 (11), 7395–7401. http://dx.doi.org/10.1063/1.354031.

Hunter, R.E., Richmond, B.M., Alpha, T.R., 1983. Storm-controlled oblique dunes of the Oregon coast. Geol. Soc. Am. Bull. 94 (12), 1450–1465. http://dx.doi.org/10.1130/0016-7606(1983)94<1450:SODOTO>2.0.CO;2.

Kocurek, G., Ewing, R.C., 2005. Aeolian dune field self-organization – Implications for the formation of simple versus complex dune-field patterns. Geomorphology 72, 94–105. http://dx.doi.org/10.1016/j.geomorph.2005.05.005.

Kocurek, G., Ewing, R.C., Mohrig, D., 2010. How do bedform patterns arise? New views on the role of bedform interactions within a set of boundary conditions. Earth Surface Process. Landforms 35, 51–63. http://dx.doi.org/10.1002/esp.1913.

Lancaster, N., 1989a. The dynamics of star dunes: An example from the Gran Desierto, Mexico. Sedimentology 36 (2), 273–289. http://dx.doi.org/10.1111/j.1365-3091.1989.tb00607.x.

Lancaster, N., 1989b. Star dunes. Prog. Phys. Geogr. 13, 67–91. http://dx.doi.org/10.1177/030913338901300105.

Lancaster, N., 1999. Geomorphology of desert sand seas. In: Goudie, A.S. et al. (Eds.), Aeolian Environments, Sediments, and Landforms. John Wiley & Sons, pp. 49–70.

Lancaster, N. et al., 2002. Late Pleistocene and Holocene dune activity and wind regimes in the western Sahara Desert of Mauritania. Geology 30 (11), 991–994. http://dx.doi.org/10.1130/0091-7613(2002)030<0991:LPAHDA>2.0.CO;2.

Madole, R.F., Romig, J.H., Aleinikoff, J.N., Vansistine, D.P., Yacob, E.Y., 2008. On the origin and age of the Great Sand Dunes, Colorado. Geomorphology 99 (1–4), 99–119. http://dx.doi.org/10.1016/j.geomorph.2007.10.006.

Marín, L., Forman, S.L., Valdez, A., Bunch, F., 2005. Twentieth century dune migration at the Great Sand Dunes National Park and Preserve, Colorado, relation to drought variability. Geomorphology 70 (1–2), 163–183. http://dx.doi.org/10.1016/j.geomorph.2005.04.014.

Merk, G. P., 1960. Great sand dunes of Colorado. In: Guide to the Geology of Colorado: Geol. Soc. America, Rocky Mtn. Assoc. Geologists, and Colorado, Sci. Soc., pp. 127–129.

Nielson, J., Kocurek, G., 1987. Surface processes, deposits, and development of star dunes: Dumont dune field, California. Geol. Soc. Am. Bull. 99, 177–186.

Reffet, E., Courrech du Pont, S., Hersen, P., Douady, S., 2010. Formation and stability of transverse and longitudinal sand dunes. Geology 38 (6), 491–494. http://dx.doi.org/10.1130/G30894.1.

Rubin, D.M., 2012. A unifying model for planform straightness of ripples and dunes in air and water. Earth-Sci. Rev. 113 (3–4), 176–185. http://dx.doi.org/10.1016/j.earscirev.2012.03.010.

Rubin, D.M., Hesp, P.A., 2009. Multiple origins of linear dunes on Earth and Titan. Nat. Geosci. 2, 653–658. http://dx.doi.org/10.1038/ngeo610.

Rubin, D.M., Hunter, R.E., 1987. Bedform alignment in directionally varying flows. Science 237 (4812), 276–278. http://dx.doi.org/10.1126/science.237.4812.276.

Rubin, D.M., Ikeda, H., 1990. Flume experiments on the alignment of transverse, oblique, and longitudinal dunes in directionally varying flows. Sedimentology 37, 673–684.

Si, H., 2002. Networks dunes in southeastern Tengger Deseert: Morphology, sediment, and dynamics. In: Lee, J.A., Zobeck, M. (Eds.), Proceedings of ICAR5/GCTE-SEN Joint Conference, Lubbock, TX, pp. 443–446.

Silvestro, S., Fenton, L.K., Michaels, T.I., Valdez, A., Ori, G.G., 2012. Interpretation of the complex dune morphology on Mars: Dune activity, modelling and a terrestrial analogue. Earth Surface Process. Landforms 37 (13), 1424–1436. http://dx.doi.org/10.1002/esp.3286.

Sweet, M.L., Kocurek, G., 1990. An empirical model of aeolian dune lee-face airflow. Sedimentology 37 (6), 1023–1038. http://dx.doi.org/10.1111/j.1365-3091.1990.tb01843.x.

Tsoar, H., 1983. Dynamic processes acting on a longitudinal (seif) sand dune. Sedimentology 30, 567–578. http://dx.doi.org/10.1016/S0070-4571(08)70798-2.

Valdez, A., 2012. Observations on dune behavior at Great Sand Dunes National Park, Colorado. Third International Planetary Dunes Workshop, Flagstaff, AZ. Abstract #7048.

Valdez, A. et al., 2007. Chapter A – Quaternery geology of the Great Sand Dunes, Quaternary Geology of the San Luis Basin of Colorado and New Mexico. US Geological Survey Open-File Report 2007-1193, pp. 1–50. http://pubs.usgs.gov/of/2007/1193/.

Warren, A., Kay, S., 1987. Dune networks. In: Frostick, L., Reid, I., (Eds.), Desert Sediments: Ancient and Modern. Geological Society Special Publication No. 35, pp. 205–212.

Wasson, R.J., Hyde, R., 1983. Factors determining desert dune type. Nature 304, 337–339. http://dx.doi.org/10.1038/304337a0.

Werner, B.T., 1999. Complexity in natural landform patterns. Science 284 (5411), 102–104. http://dx.doi.org/10.1126/science.284.5411.102.

Werner, B.T., Kocurek, G., 1997. Bed-form dynamics: Does the tail wag the dog? Geology 25 (9), 771–774. http://dx.doi.org/10.1130/0091-7613(1997)025<0771:BFDDTT>2.3.CO;2.

Zhang, W., Qu, J., Dong, Z., Li, X., Wang, W., 2000. The airflow field and dynamic processes of pyramid dunes. J. Arid Environ. 45 (4), 357–368. http://dx.doi.org/10.1006/jare.2000.0643.

Zhang, D., Narteau, C., Rozier, O., Courrech du Pont, S., 2012. Morphology and dynamics of star dunes from numerical modelling. Nat. Geosci. 5, 463–467. http://dx.doi.org/10.1038/ngeo1503.